Automation in Construction 91 (2018) 155–165

Contents lists available at ScienceDirect

Automation in Construction

journal homepage: www.elsevier.com/locate/autcon

Floor cleaning robot with reconfigurable mechanism

Veerajagadheswar Prabakaran[a,*], Mohan Rajesh Elara[a], Thejus Pathmakumar[a], Shunsuke Nansai[b]

[a] Engineering Product Development, Singapore University of Technology and Design, 487372, Singapore
[b] Department of Advanced Machinery Engineering, Tokyo Denki University, Tokyo 120-8551, Japan

ABSTRACT

Although several precedents have demonstrated the benefits of using floor cleaning robots for the maintenance of constructed buildings, traditional platforms suffer from a series of performance issues. One major factor that contributes to their performance deficit is their fixed morphology design, which highly constrains their navigation and access. To this end, a novel Tetris-inspired reconfigurable floor cleaning robot called hTetro is presented in this paper. The developed robot is capable of reconfiguring its morphology to any of seven one-sided tetrominoes in response to its perceived environment to maximize its coverage area. This paper presents the coverage area performance of the hTetro robot and systematically benchmarks its performance with two commercially available fixed morphology robot platforms. Our experiments indicate that hTetro achieves significantly higher coverage performance than the other platforms due to its shape-shifting ability in response to navigating its environment.

1. Introduction

The maintenance of constructed buildings typically involves a series of endless routines consisting of dull, dirty, time-consuming and tedious tasks such as floor cleaning. Over the last two decades, researchers have made huge efforts to develop and deploy autonomous cleaning robots for maintenance of constructed buildings. Such efforts have materialized into robotic products significantly improving productivity and quality of life. Floor cleaning robots are likely to be an elemental part of every household in the near future, and it is expected to reach a market value of USD 2.50 Billion by 2020 [1]. Successful market players include the iRobot Roomba, Neato XV–II, Samsung Powerbot, Bobsweep bobi, Miele scout, Moneual RYDI and infinuvo Clean Mate. Often characterized by circular and 'D' shaped morphologies, such robots can autonomously map their environment using onboard sensors and traverse a defined floor space. The various aspects of floor cleaning robots, including mechanism design, human interaction, and autonomy, have been researched in depth over the last two decades. For example, Gao et al. present a floor cleaning robot with Swedish wheels that attains highly efficient locomotion in crowded places such as railway stations and airports [2]. In another work, Kakudou et al. presents a novel staircase cleaning robot equipped with L-shaped legs on both sides of its body frame for staircase ascent and descent locomotion [3].

An innovative neural network approach towards robot autonomy is conceived and validated by Yang and Luo in [4]. Their method covers path planning and obstacle avoidance for cleaning robots in dynamic environments. In their approach, an evolving action scene is generated by a neural network, and the robot's last position is used for path planning. Siop et al. [5] discuss a new technique called triangular cell map representation that helps a cleaning robot identify shorter paths, offering increased navigational flexibility compared with rectangular cell maps. They also propose complete coverage navigation and methods for map construction to enable a cleaning robot to perform navigation on an entire workspace given basic information regarding its environment. In [6], the authors experimentally investigate the coverage performance of a chaotic autonomous mobile robot. The proposed approach uses a microcontroller to generate a chaotic bit sequence and suitable robot trajectory. A SLAM-based approach for improving the coverage of floor cleaning robots is presented in [7]. This method uses a fusion of magnetic field and odometry data to synthesize an accurate map for efficient autonomous navigation and improved area coverage.

Several human-robot interaction studies involving floor cleaning robots have been reported in recent years. Fink et al. [8] report on an ethnographic study of floor cleaning robots in separate households over a period of approximately six months. In their study, user perception, usage analysis, and social activities with respect to cleaning robots are extensively studied. Sakamoto et al. present a stroke gesture-based computer screen interface for interacting with a floor cleaning robot [9]. Their experiments demonstrate the validity of the proposed interface in controlling a cleaning robot and capturing multiple views from ceiling cameras. Luo and Yang propose multi-robot cooperative

* Corresponding author.
E-mail addresses: prabakaran@sutd.edu.sg (V. Prabakaran), rajeshelara@sutd.edu.sg (M.R. Elara), nansai@ctrl.fr.dendai.ac.jp (S. Nansai).

https://doi.org/10.1016/j.autcon.2018.03.015
Received 31 July 2017; Received in revised form 14 February 2018; Accepted 8 March 2018
Available online 22 March 2018

sweeping based on a bio-inspired neural network approach [10]. The authors use multiple cleaning robots to study the complete coverage and path planning issues associated with unstructured workspaces. Another significant study [11] presents a cellular decomposition method to divide a cleaning area into cells and provide an effective coverage plan to two indoor floor cleaning robots over the cells.

With the market becoming increasingly flooded with floor cleaning robotic products, interest in benchmarking various robotic systems has also grown. A set of performance metrics for autonomous cleaning robots is reported in Rhim et al. [12], who define autonomous mobility, dust collection, and operation noise as critical performance indices for the majority of cleaning robots. Wong et al. propose two metrics to capture robotic cleaning performance and coverage efficiency and validate them with real-world trials [13]. This study also presents experimental approaches using computer vision techniques to benchmark the performance of cleaning robots. Zheng et al. in [14] present the evaluation of path planning algorithm for multiple floor cleaning robot platforms using a Mocap system. This work also put forward and validate three simple metrics to benchmark the overall performance of the area coverage algorithm. Prassler et al. in [15] share their experiences in organizing the First International Contest for Cleaning Robots, which took place jointly with IROS 2002 in Lausanne, Switzerland. This work provides extensive details on the efforts made to ensure a well-defined setup, which could be replicated for every run of the competition contest and participating team. Also, this work put forward a set of fair criteria for benchmarking the performance of the participating cleaning robots. Although numerous studies in the literature demonstrate the use of floor cleaning robots for the maintenance of constructed building spaces, conventional robots suffer from a series of performance issues that curtail their full potential. One major factor that contributes to the performance degradation associated with cleaning robots is their fixed morphology design, which highly limits their navigation and access. One viable approach to overcome this bottleneck is to develop a next-generation cleaning robot that can reconfigure its morphology to maximize cleaning performance.

Since the early 1980s, the design philosophy of reconfiguration has been actively considered and applied to robotic systems. As a result, a number of reconfigurable robotic platforms have been proposed. It is a proven fact that reconfigurability has widened the scope and diversity of robot design. In our previous work, we classified reconfigurable robots broadly into three categories, namely, inter-, intra- and nested reconfigurable platforms [16]. An intra-reconfigurable robot comprises a combination of sensors, actuators, mechanical parts, power and a controller and acts as a single entity capable of changing its internal morphology. Precedents to this end include a versatile robot that can switch between amphibious and terrestrial gait mechanisms [17], an anthropomorphic robotic hand capable of reconfiguring its palm to generate changeable topologies [18], a reconfigurable, underactuated, legged robot that generates a variety of locomotion gaits [19] and a reconfigurable bio-inspired robot that can switch between three locomotion modes: rolling, climbing and crawling [20]. Robots in the inter-reconfigurable category consist of modular homogeneous or heterogeneous units that can assume a variety of morphologies via assembly and/or disassembly processes [21]. One example of an inter-reconfigurable robot is Sambot [22]. Multiple Sambots can assemble and disassemble to form new robot morphologies. Another case involves an underwater platform capable of splitting into independent rigid modules and joints to swim like an eel [23]. In [24], a robot is described as being capable of multiple locomotion modes via assembly and disassembly processes. CEBOT, Poly Bot, Crystalline, M-TRAN, ATRON, Molecube and CKBot are other relevant examples of inter-reconfigurable robots. Robots in the third class, nested reconfigurable robots, are capable of performing both inter- and intra-reconfigurability, thereby expanding their reconfiguration options. Hinged-Tetro, presented in [25], is a nested reconfigurable robot capable of reconfiguring its morphology as an individual as well as assembling/disassembling itself to generate global morphologies. In spite of the fact that numerous studies including our prior research efforts in the literature address reconfigurable robotics, they are largely limited to mechanism design, often with a loose connection to an end application. In addition, none of the previous work in reconfigurable robotics targets the floor cleaning task, which presents significant opportunities for research and development.

A novel Tetris-inspired reconfigurable floor cleaning robot called hTetro is presented in this paper. hTetro is based on the theory of the hinged dissection of polyominoes. The developed robot is capable of transforming itself into any of seven one-sided tetrominoes formed in relation to the navigating environment with an objective of maximizing the coverage area. The major challenges encountered during the development of our hTtero robot were its reconfigurable mechanism design, the integration of vacuum modules, and translating the theoretical design into a physical mechanism. This paper summarizes all these aspects and concludes with experimental results that validate the area coverage efficiency of the proposed robot in comparison with two conventional fixed morphology platforms. hTetro represents an initial design towards building a self-reconfigurable floor cleaning robot that can autonomously reconfigure its morphology by sensing its environment to maximize floor coverage.

This paper is organized as follows: Section “Design Principle of the hTetro Robot” introduces the principles of polyominoes and hinged dissection. Section “h Tetro System Architecture” presents the hardware and software building blocks of the hTetro platform and covers the module-wise description of the reconfigurable base, mobility unit, and cleaning modules. Section “Experiments” presents the experimental setup and methods and provides details on the identified performance metrics. Section “Results and Analysis” presents a detailed analysis of the results, validating the coverage performance of hTetro robot in comparison with two commercial platforms. Finally, the “Conclusion” section concludes this study and discusses future research directions.

2. Design principle of the hTetro robot

Polyominoes are the inspiration for the design of our hTetro robot and its reconfiguration strategies. Polyominoes are two-dimensional geometric structures joining one or more similar squares edge to edge in varying arrangements. A polyomino consisting of n squares is termed as n-omino or n-polyomino [26]. A polyomino with a combination of two congruent squares is called a domino, a combination of three squares forms a triomino, and a combination of four squares forms a tetromino, as shown in Fig. 1. Polyominoes have been popularly adopted in several entertainment puzzles since the 18th century [27].

Polyominoes can be classified as free polyominoes, one-sided polyominoes, and fixed polyominoes based on their geometry and chirality. The free polyomino can be considered as a subset of the n-polyomino domain such that each element exhibits chirality in terms of its spatial orientation. One-sided polyominoes exhibit similarity in terms of their geometry, irrespective of right-angled rotational transformations. Unlike free polyominoes, one-sided polyominoes do not show chirality. Hence, the mirror image of the structure of each one-sided polyomino can be treated as another distinct element belonging to the same subset. Fixed polyominoes can be treated as another subset of the polyomino domain wherein each element (lattice animal) is distinct in terms of its rotational and flip transformations. Based on [28], single one-sided, single free and two fixed dominoes form the domino group of polyominoes. Similarly, two free, two one-sided, and six fixed triominoes (3-ominoes) form the triomino group. In [28] it is documented that, for a group of tetrominoes, there exists five free, seven one-sided, and nineteen fixed tetrominoes. Because the tetromino accommodates a large number of polymorphs, we adopted the tetromino geometrical structure as the morphology of our self-reconfigurable cleaning robot. Our hTetro platform is capable of reconfiguring its morphology into any of seven one-sided tetrominoes in response to its perceived environment

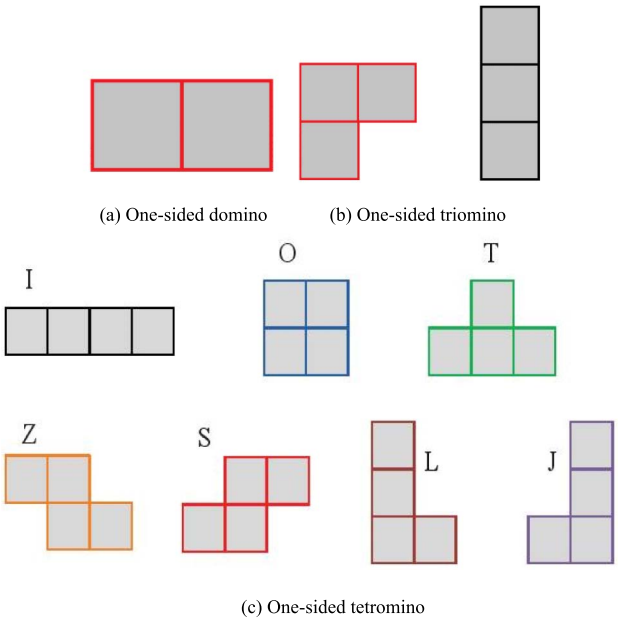

Fig. 1. Examples of polyominoes.

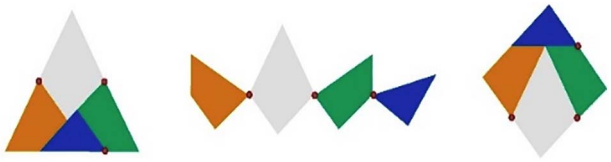

Fig. 2. Hinged dissection.

with the objective of achieving optimal coverage area and, thereby, cleaning performance. The strategy adopted in our research is analogous to the gap filling approach in conventional Tetris games. Fig. 1(c) illustrates the seven free tetromino structures adopted for dynamic morphology generation in the hTetro robot.

The main challenge in designing the hTetro robot was the placement of hinged dissection points to enable shape-shifting from one configuration to another. A hinged dissection is a geometric methodology that divides a planar structure into a finite number of pieces connected by "hinged" points in such a way that a new shape can be created by rearranging the dissected pieces without breaking the chain structure formed by the hinged points [29]. Fig. 2 illustrates the hinged dissection approach. Several studies have reported on the concept of hinged dissection since 1984. For instance, hinged dissection can be used to transform an equilateral triangle into a polygon [30]. In addition, [31] demonstrates the usage of 3D hinged dissection for polyhedra involving connected 3D solids formed by merging several rigid copies of the same polyhedron along identical faces. In [32], a hinged dissection based approach to pattern generation is presented. The patterns are created so that, when they are rotated from one shape of the dissection to another, the patterns also change along with the shapes.

The current literature on hinged dissection is generally confined to solving a typical dissection problem in planar and spatial geometry. We presented an innovative application of hinged dissection in a previous study wherein we developed a nested reconfigurable robot module called hinged-Tetro to prove that LLR or LLL hinged dissection can be used to achieve all seven one-sided tetrominoes [25]. Our preliminary efforts to develop floor cleaning robot using hinged dissection principle is detailed in [33]. In this paper, we build on our past work towards quantifying the performance superiority of our shape-shifting approach to floor cleaning robots. For the work presented in this paper, we adopted the LLR hinged dissection shown in Table 1 to enable its shape-shifting capabilities.

Table 1
Hinged dissection of tetrominoes in LLR configuration.

Hinged Dissection	O	T	Z	S	L	J
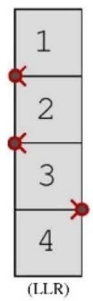 (LLR)	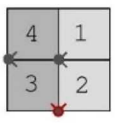 1) ${}^{2}R_{3} = -180^{0}$	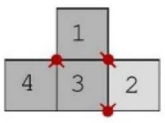 1) ${}^{2}R_{3} = -180^{0}$ 2) ${}^{3}R_{4} = +180^{0}$ 3) ${}^{2}R_{1} = +90^{0}$	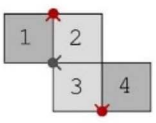 1) ${}^{2}R_{1} = +180^{0}$ 2) ${}^{3}R_{4} = +180^{0}$	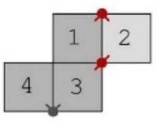 1) ${}^{2}R_{1} = +180^{0}$ 2) ${}^{2}R_{3} = -90^{0}$	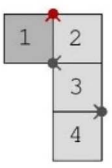 1) ${}^{2}R_{1} = +180^{0}$	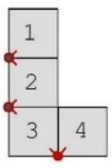 1) ${}^{3}R_{4} = +180^{0}$
Robot Prototype (LLR) I Configuration 	O Configuration 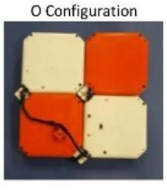	T Configuration 	Z Configuration 	S Configuration 	L Configuration 	J Configuration 

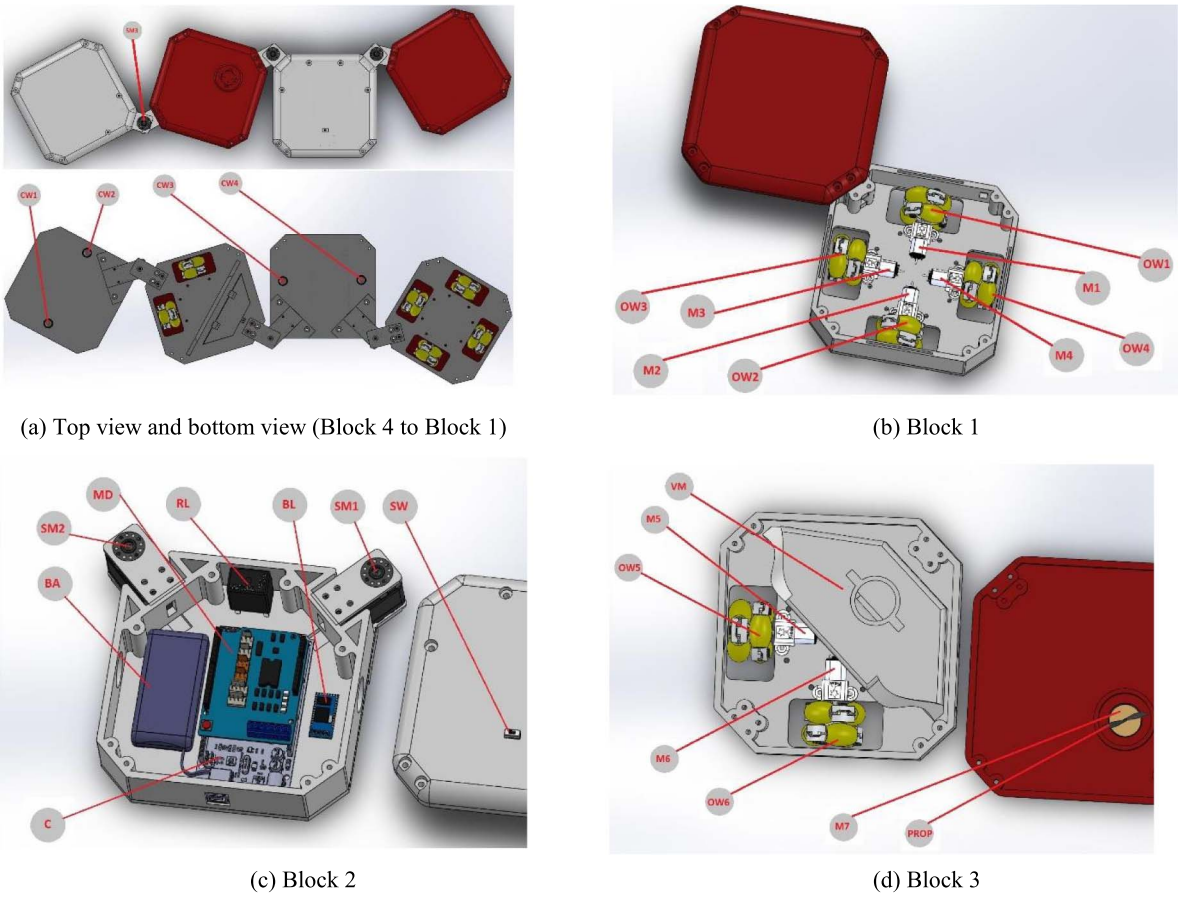

(a) Top view and bottom view (Block 4 to Block 1)

(b) Block 1

(c) Block 2

(d) Block 3

Fig. 3. hTetro's CAD and the component used in each block.

3. hTetro system architecture

As shown in Fig. 3(a), our hTetro robot consists of four square blocks with three (LLR) hinged actuation points. Because our hTetro robot is compact, each block is assigned a particular function. For instance, Block 1 is responsible for mobility functions, Block 2 houses the control and power modules and Blocks 3 and 4 hold the cleaning functions.

3.1. Mechanical design

The enclosure of the robot has four square blocks connected by three active hinges. Each block of the hTetro robot has the following dimensions: 140 mm length, 140 mm width and 55 mm height. The blocks are designed with no sharp edges to avoid collisions between the blocks during transformation. The walls of the robot enclosure are fabricated in honeycomb patterns with a thickness of 4 mm to minimize weight and maximize tensile strength. The total weight of the hTetro robot, including all its peripheral devices, is approximately 3 kg. The hTetro robot is equipped with a set of six motors for mobility and three motors for transformation. For the robot's locomotion, six Pololu DC geared motors with a working voltage of 7.4 V are used. As it is responsible for mobility, four of the six DC motors (M1 to M4) are mounted in Block 1. The remaining two motors (M5 and M6) are placed in Block 3, which ensures smooth navigation for the hTetro robot. Each motor is mounted on a spring suspension to overcome bumps and traverse uneven terrain. Because we use multiple DC motors for locomotion under seven different robot morphologies, each motor is programmed to operate differently under specific configurations. For instance, motors M1, M2 and M5 are used for forward and reverse motions in the 'I', 'S', and 'J' configurations and perform a lateral motion in the 'O', 'T', 'Z', and 'L' configurations. Motors M3, M4 and M6 act in the opposite manner. We use omnidirectional wheels (OW1-OW6) for our hTetro robot to realize multi-directional locomotion. In addition, four caster wheels (CW1-4) are mounted in Blocks 2 and 4 to improve robot's mobility. Seven different configurations of hTetro can be realized by controlling three actuated hinged points. Three Herkulex DRS-0101-7 V smart servos activate the hinges and control reconfigurability. The smart servo motors can rotate to a maximum of 270 degrees and have an inbuilt encoder feedback system for precise control. The servos SM1 and SM2 attached to Block 2 (Fig. 3(c)) act as an anchor and drive both Block 1 and Block 3. SM3 is placed in Block 4 (see Fig. 3(a)) and drives Block 4. Each servo has a stall torque of approximately 12 kg, which allows the motor to lock the positions of the blocks at the end of every transformation. When the robot starts moving, the blocks are automatically locked to maintain the morphology of the robot throughout its locomotion. Additionally, a separate vacuum module VM is integrated into Block 3 (Fig. 3(d)), wherein a high RPM motor M7 is used for realizing the vacuuming function shown in Fig. 3(d), which performs vacuuming functions and collects dirt particles. The path of the suction module is designed to avoid vacuum or dust leakage during cleaning.

The locomotion and transformation of the robot are achieved by coordinating its actuators and microcontroller. An Arduino

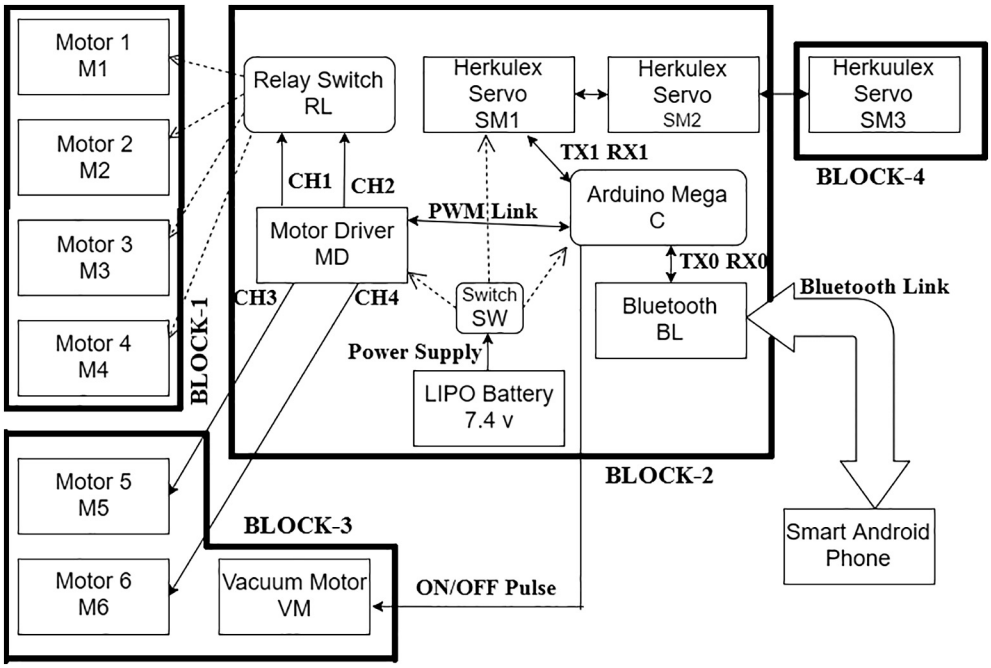

Fig. 4. System architecture of the hTetro robot.

Atmega2560 16-Bit microcontroller is used to control the robot's locomotion, shape transformation and human-robot interaction. It has 54 digital input/output pins, 16 analog inputs, 4 UARTs (hardware serial ports), a 16 MHz crystal oscillator, a USB connection, a power jack, an ICSP header, and a reset button. The microcontroller is located in the second block of our robot, as seen in Fig. 3(b). The microcontroller is programmed to carry out 3 major functions: (1) generate control signals to the motor driver unit MD, which controls the speed of the M1- M6 motors, (2) control signal generation for the servo motors (SM1-SM3) for reconfiguration and receive feedback from them and (3) receive user commands from a remote smartphone device. The motor driver used has four 4 H-Bridges TB6612 chipset provides 1.2A per bridge (3A for brief 20 ms peaks) with thermal shutdown protection, internal kickback protection diodes, and can run motors on 4.5 VDC to 13.5 VDC with individual 8-bit speed selection. For each of the six motors, the speed and time period for the motor's rotations are defined by pulse-width modulation (PWM) signals from the microcontroller. Because the robot is deployed with six motors, a 5v DPDT (double pole double through) relay switch, RL, with 1A of switching load current is used to switch between the motors for different configurations. In every transformation, the microcontroller gives a serial command (trough RX1-TX1 pin) to SM1-3, and at the end of the transformation, the controller receives feedback on the motor's position from SM1-3 to cross-check its position. The controller receives wireless commands from a remote user (through RX0-TX0 pins) to perform a task, for which an HC-06 (5 V) Bluetooth device BL with 2.4 GHz ISM band frequency is used. The entire circuit is powered using a LIPO battery BA with 7.4 V and 900 mAh capacity. A toggle switch (SW) is connected to the main power supply branch, which enables convenient circuit assembly and breakage. The detailed system architecture of electrical connections is shown in Fig. 4. Even though our hTetro robot would require increased number of actuators and computational needs to realize the shape shifting features in comparison to traditional floor cleaning robotic platforms. The performance superiority in area coverage that comes with our hTetro platform largely outweighs the additional needs for actuators and computational needs. In addition, the advancement of actuation and computing technology over the last two decades have resulted in improved sophistication, small footprint, high precision and lower cost of such systems.

3.2. Software design

hTetro receives manual commands to achieve transformations between seven tetromino morphologies. The user can choose the most appropriate morphology for the perceived environment with the objective of achieving maximum coverage. The current hTetro prototype is an initial design in the direction of an autonomous shape-shifting robot requiring no human intervention. A mobile application was developed and installed on an Android/IOS smartphone device. The developed application contains navigation and seven transformation buttons on the control page as shown in Fig. 5 (right). Before sending commands from the developed app, a Bluetooth connection must be established between the application and the Bluetooth device BL mounted on the hTtero. The user can select the required device from the “Available Device” box as shown in Fig. 5 (center); this box appears after selecting the “Plus” symbol in Fig. 5 (left). Once a connection has been established, the robot control page appears onscreen, and the hTetro robot can react to the commands received from the application. In the application, the arrow keys are used for navigational commands, and the play icon is used to pause or start the current operation. The ON and OFF buttons are used to perform the vacuuming function.

4. Experiments

We evaluated the performance of our hTetro robot against two commercially available fixed morphology robots under two experimental conditions. In the first set of experiments, the robots were deployed to clean a fixed area with a single chair as an obstacle. The experiment was performed using ten different types of chairs with five trial runs of each chair. The coverage areas of hTetro and the other two commercially available robots were computed using all ten chairs, and we compared their coverage performance. The chair types used in the

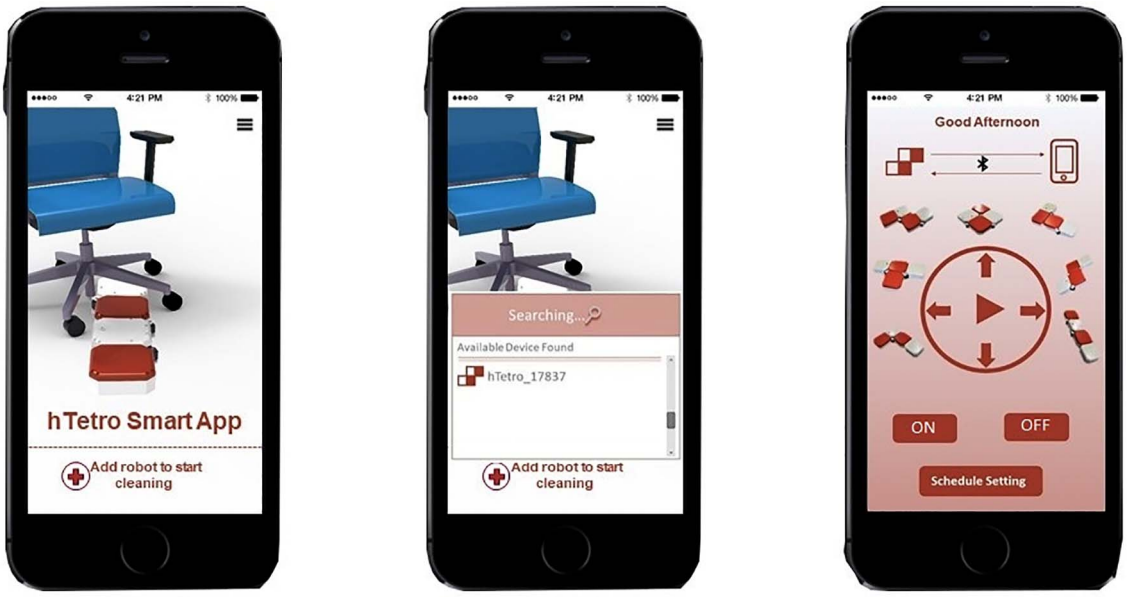

Fig. 5. hTetro graphical user interface.

Fig. 6. Chair types used in the experiments.

first experiment are shown in Fig. 6. Each chair was assigned a complexity rank based on its ease of accessibility to the cleaning robots. Due to the fact that a chair with more legs occupies greater space, thereby decreasing its accessibility to cleaning robots, a chair's complexity rank was defined by a score of 1–10 based on its number of legs and the distance between them. During the second set of experiments, hTetro's performance was compared with two fixed morphology robots with distinct morphologies in an office-like environment. One of the commercial robot platforms was circular and the other was 'D'-shaped. These two fixed morphologies are the most commonly encountered morphologies in existing commercial floor cleaning robots. Within the same experimental setting, the coverage area performance of the considered robots was computed across varying degrees of obstacle density. To standardize the comparison, the commercial robots were reverse engineered to be manually controlled using an Android smartphone application. The two fixed morphology experimental platforms used in our experiments are shown in Fig. 7. The experimental testbed consisted of a predefined floor area to be cleaned, support frames, an image acquisition device and a vision based benchmarking scheme that computed the coverage area automatically by tracking the robot within the operating space.

4.1. Predefined floor area

The predefined floor area considered in this paper is a rectangular, polished laboratory floor with boundaries defined by extendable metal

Specifications of Fixed morphology robots

Size of the Circular Robot	280 (Diameter) X 75 (height) mm
Size of the 'D' shaped Robot	290 (Diameter) X 76 (height) mm

Fig. 7. Experimental fixed morphology platforms.

Fig. 8. Experimental setup after removing the seat of the chair.

frames. The surface area of the cleaning space can be varied by reconfiguring the arrangement of the extendable metal frames. For the first set of experiments, we used an area of 93 cm × 168 cm, and, for the second set of experiments, we used an area of 200 cm × 168 cm. A camera was placed perpendicular to the cleaning surface with a fixed focal length. The altitude for fixing the camera was selected so that the entire cleaning area was covered in the camera's field of view. We also ensured that the movement of the robot would not be eclipsed by any of the obstacles. For instance, the seats of the chairs were removed so that the benchmarking scheme could track the robot's movement under chairs (see Fig. 8).

4.2. Support frame

Using a T-slot aluminum extrusion profile, a parallelepiped structure was built to provide vibration-immune support for the camera mount over the cleaning space (see Fig. 9). The support frame has the following dimensions: 2000 mm length, 2000 mm breadth, and 2500 mm height. The camera was fixed exactly at the midpoint of the upper face of the supporting frame.

4.3. Image acquisition device

We used a digital HD camcorder with a resolution of 2.07 megapixels as an image acquisition device. The employed camcorder has a built-in storage memory for storing all the recorded raw video footage. The camera used has a frame rate of 24 fps with a fixed focal length of 61 mm. The test arena was manually focused to record the experimental trials of each robot's cleaning process. The raw video files were then

Fig. 9. Complete experimental setup.

copied to a computer and converted into mp4 files. The converted files were then used as the input to a vision based benchmarking scheme.

4.4. Vision-based benchmarking scheme

The vision-based benchmarking scheme automatically computes the total area coverage performance of the tested robots by continuously tracking the area covered. The first processing step saves the first frame as a reference image for track map generation. The second phase of the benchmarking scheme detects the deployed robot and its position in every frame. The third step generates a track map by plotting the identified position of the robot on the reference image. Coverage area performance is then calculated using the overlapped positions of the robot in the reference image. This scheme is completely implemented in MATLAB (R2015a). Because the circular-shaped commercial cleaning robot possesses a round geometry, we used Hough transformation-based circle detection to determine the position of the geometric center of the robot. Once the robot's center was identified, a green colored circle with the same radius was replicated on the reference image corresponding to the center coordinates to generate the tracking map. Because hTetro has dynamic morphology, we used color-based blob detection and tracking approach wherein four red blobs detect the hTetro platform in each video frame. Using the detected blobs, the hTetro's coverage area can be identified, and green squares are plotted on the reference image over the complete video sequence. After generating the tracking maps on the reference images, the percentage of the area covered was calculated using Eq. (1) for the first set of experiments and Eq. (2) for the second round of experiments. In Eqs. (1) and (2), the pixel area of the test robot can be computed by identifying the green colored pixels on the track map on the reference image. The images were purely used for benchmarking purposes to compare the area coverage performances of the considered robotic platforms, and our future work is set to explore the use of these images for global and

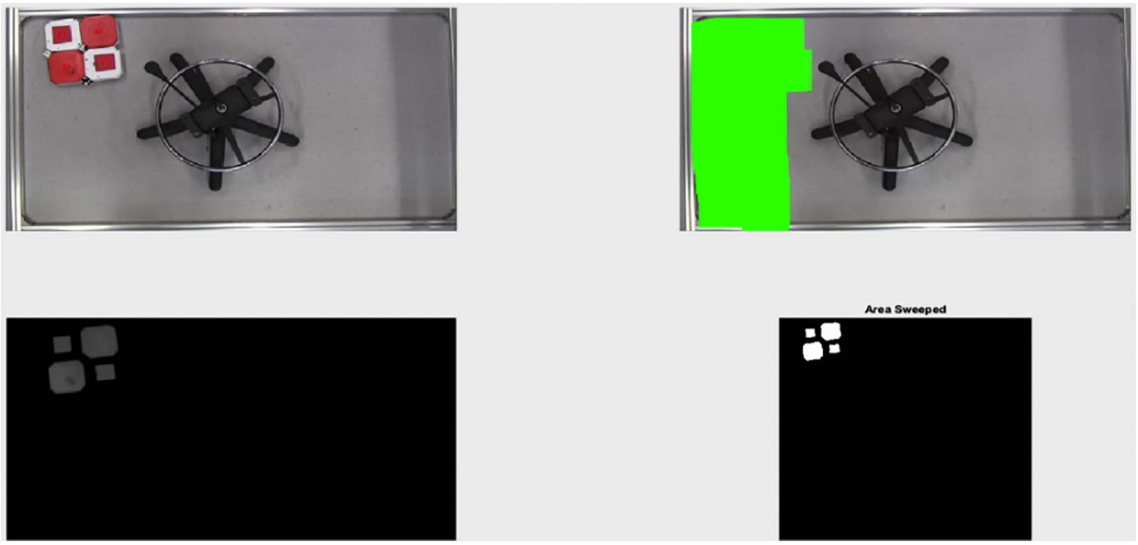

Fig. 10. Vision based benchmarking scheme for processing video with hTetro. (For interpretation of the references to color in this figure, the reader is referred to the web version of this article.)

(a) Vision based benchmarking scheme for processing video with the circular-shaped robot.

(b) Vision based benchmarking scheme for processing video with the D-shaped robot.

Fig. 11. Vision based benchmarking scheme for processing video with fixed morphology robots. (For interpretation of the references to color in this figure, the reader is referred to the web version of this article.)

local path planning.

$$\textit{Percentage of area covered} = \frac{\text{Pixel area of the robot}}{\text{Total pixel area of the testing field}} \times 100 \tag{1}$$

$$\textit{Percentage of area covered} = \frac{\text{Pixel area of the robot}}{\text{Total pixel area of the testing field} - \text{Total pixel area of the obtacles}} \times 100 \tag{2}$$

5. Results and analysis

The experimental trials were started by placing the chairs and test robot at their initial positions. After the tests were completed, the recorded videos were post-processed to generate a track map using a stepwise vision based benchmarking scheme. This scheme used to track the commercial circular-shaped robot uses three steps to generate the robot's track map. The first step is a filtering process in which the frames are passed through a sliding window median filter for suppressing the effect of noise. The next step is to find the circle presented in every frame using a Hough transformation as shown in Fig. 11a (right), which also identifies the center of the circular-shaped robot. In the third step, a green colored circle with the same radius is duplicated on the reference image using the detected center as shown in Fig. 11a (left). These steps continue to the final frame, converting the reference image into a track map of the considered robot. The benchmarking scheme used for the hTetro and D-shaped robots comprised five steps to generate a track map. The first step is the filtering process used in the previous benchmarking scheme for the circular-shaped robot. In the second step, the red components in the image are separated by extracting the red layer from the RGB color space representation of the filtered image as shown in Fig. 10 (bottom right). Once the red layer is extracted, in the third step, a binary image is generated by mapping the 8-bit encoded pixel values in the red layer matrix to either zero or one based on a fixed threshold. The binary image generated in this manner

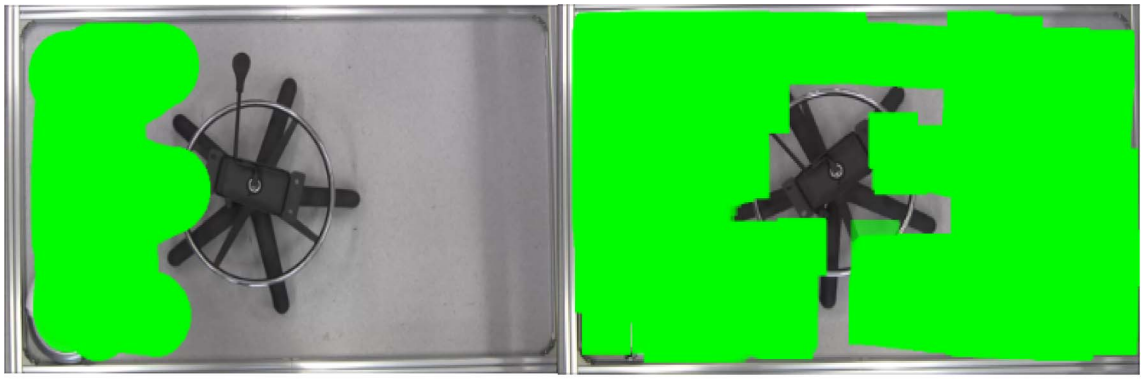

(a) Track map of the circular-shaped robot. (b) Track map of the hTetro robot.

(c) Track map of the D-shaped robot.

Fig. 12. Resulting tracking maps on the reference image for the circular-shaped robot (a), hTetro (b) and the 'D'-shaped robot (c) around a piece of furniture ranked as 10. (For interpretation of the references to color in this figure, the reader is referred to the web version of this article.)

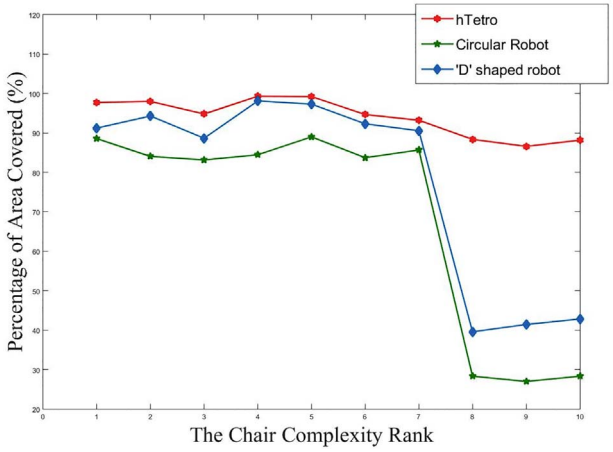

Fig. 13. Percentage of the covered area of all the robots for first set of experiments.

contains white blobs that represent the presence of red-colored objects as shown in Fig. 10 (bottom left). The next step is blob detection and analysis of the binary image using a computer vision toolbox. To improve efficiency with prior knowledge and avoid false alarms, we excluded tiny blobs with an area of less than or equal to 200 pixels. The centroid obtained from the remaining blobs represents each block of the hTetro and 'D'-shaped robots as shown in Fig. 10 (top left) and Fig. 11b (left). The output of the previous step becomes the coordinates of the centroids. Using the detected blobs, the hTetro and D-shaped robots' areas are identified, and green squares are plotted on the reference image over the complete video sequence as shown in Fig. 10 (top right) and Fig. 11b (right).

Fig. 12(a), (b) and (c) illustrates the track map images of all the considered robots in the first set of experiments. The green colored shading represents the area covered by the robots. The percentage of the area covered was calculated with Eqs. (1) and (2). Fig. 13 shows the average percentage of the area covered for all the tested robots under each ranked chair in the first set of experiments. The processed images clearly indicate that hTetro has a significantly larger coverage area than the fixed morphology robots. Using its shape-shifting mechanism, hTetro covered more than 80% of the testing area of the highly-rated chair with a score of greater than eight, whereas both of the fixed morphology robots covered less than 50% of the set area. The overall coverage performance of hTtero across all the chair types was greater than 95%, whereas the circular-shaped robot achieved 68.27% coverage, and the 'D'-shaped robot achieved 77.64% coverage.

In the second scenario, the boundaries of the testing field were extended, and the camera lens was adjusted to cover a new enlarged field of area 3.36 m^2. We created a mock office setup with six static obstacles inside the test scenario as shown in Fig. 14. The obstacle density was calculated by computing the total pixels occupied by all the obstacles placed in the testing field. The track maps of all the considered robots with an obstacle density of 6% are shown in Fig. 15(a), (b) and (c). The percentage of the area covered in the second set of experiments was calculated only for the accessible area (ignoring the area occupied by the obstacles placed inside the scenario). The obstacle density was gradually increased, and the associated coverage performance of the robots was captured experimentally. Fig. 15(d), (e) and (f) gives the coverage performance of the robots with an obstacle density of 66%.

(a) (b)

Fig. 14. Testbed setup for the second set of experiments before (a) and after (b) removing the top surface of the furniture.

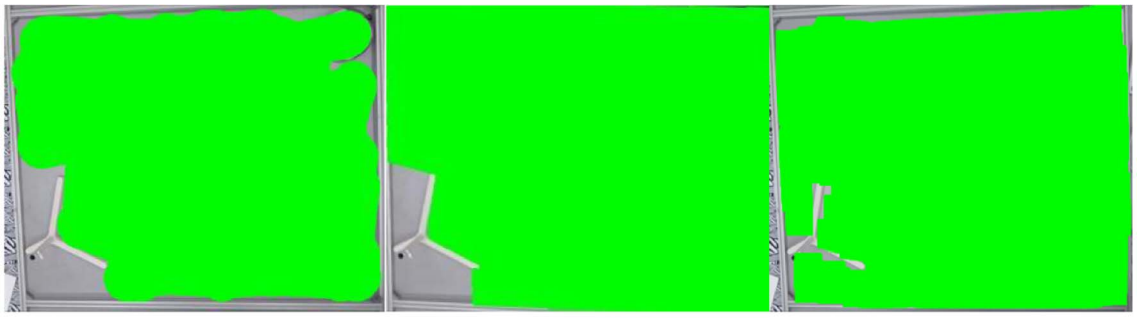

(a) Track map of circular-shaped robot with 6% obstacle density.

(b)Track map of D-shaped robot with 6% obstacle density.

(c) Track map of hTetro robot with 6% obstacle density.

(d) Track map of circular-shaped robot with 66% obstacle density.

(e)Track map of D-shaped robot with 66% obstacle density.

(f) Track map of hTetro robot with 66% obstacle density.

Fig. 15. Resulting tracking map on the reference image for the circular-shaped robot (a & d), the 'D'-shaped robot (b & e) and hTetro (c & f), under increasing obstacle density.

The results indicate a significant drop in performance for both of the fixed morphology robots with increasing obstacle density. Fig. 16 shows the average percentage of the covered area for all the tested robots based on five runs for each level of obstacle density. The results indicate the superior coverage performance of hTtero in comparison with both the fixed morphology robots across all the experimental cases. The higher coverage performance of hTetro is mainly attributed to its ability to navigate narrow corridors and tight spaces by changing its morphology. The average coverage area for hTetro in the second set of experiments was 94.56%, whereas the average coverage area of the circular- and 'D'-shaped robots were only 80.52% and 85.98%, respectively.

6. Conclusion

In this paper, we have presented a novel reconfigurable Tetris-inspired floor cleaning robot called hTetro that implements the hinged dissection of polyominoes. We introduced the mechanical design, electrical system and HMI modules of the hTetro robot and successfully validated its ability to transform between any of seven one-sided tetromino morphologies to maximize floor coverage. Experiments were performed in two different settings to systematically compare the coverage area performance of the developed hTetro robot with two commercially available circular and 'D'-shaped fixed morphology robot platforms. We tracked the test robots using an overhead camera on top of a constructed testbed to generate the robots' track MAPS. The track

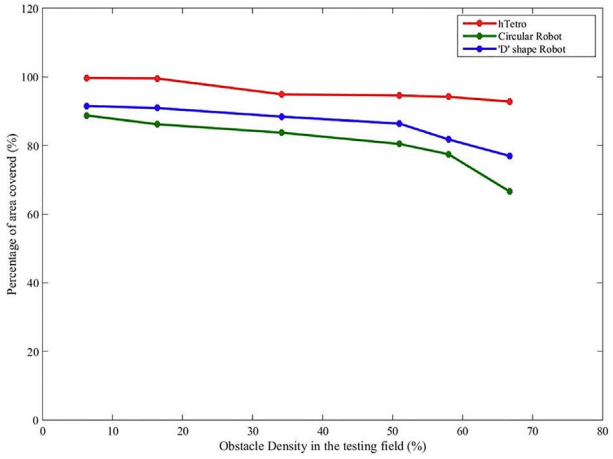

Fig. 16. Percentage of area covered in the second set of experiments.

maps generated from each set of experiments were post-processed to measure the area covered by the robots. In both sets of experiments, the hTetro robot exhibited a significant performance advantage in terms of floor coverage area due to its ability to assume optimal morphologies while navigating its environment.

Future research work is set to mainly focus on the following areas: the first is to integrate range and bump sensors to enable autonomous navigation in the hTetro robot. The second is to study the application of Polyomino tiling theory towards facilitating global path planning through automatic generation of global tiling set required to cover a defined space. Moreover, we intend to implement highly adaptive locomotion control that allows for smooth trajectories at low computational costs across all seven configurations.

References

[1] Marketsandmarkets, Cleaning Robot Market by Type, Product (Floor-cleaning Robot, Lawn-cleaning Robot, Pool-cleaning Robot, Window-cleaning Robot), Application (Residential, Commercial, Industrial, Healthcare), and Geography - Global Forecast to 2023, marketsandmarkets.com, (2018, January) Retrieved Feb 01, 2018, from https://www.marketsandmarkets.com/Market-Reports/cleaning-robot-market-22726569.html.

[2] X. Gao, K. Li, Y. Wang, G. Men, D. Zhou, K. Kikuchi, A floor cleaning robot using Swedish wheels, IEEE International Conference on Robotics and Biomimetics (ROBIO), IEEE, 2007, , http://dx.doi.org/10.1109/robio.2007.4522487.

[3] T. Kakudou, K. Watanabe, I. Nagai, Study on mobile mechanism for a stair cleaning robot-design of translational locomotion mechanism, Control, Automation and Systems (ICCAS), 11th International Conference on, IEEE, 2011, October, pp. 1213–1216 (ISBN: 978-8993215038).

[4] S.X. Yang, C. Luo, A neural network approach to complete coverage path planning, IEEE Trans. Syst. Man Cybern. B Cybern. 34 (1) (2004) 718–724, http://dx.doi.org/10.1109/tsmcb.2003.811769.

[5] J.S. Oh, Y.H. Choi, J.B. Park, Y.F. Zheng, Complete coverage navigation of cleaning robots using triangular-cell-based map, IEEE Trans. Ind. Electron. 51 (3) (2004) 718–726, http://dx.doi.org/10.1109/tie.2004.825197.

[6] C.K. Volos, I.M. Kyprianidis, I.N. Stouboulos, Experimental investigation on coverage performance of a chaotic autonomous mobile robot, Robot. Auton. Syst. 61 (12) (2013) 1314–1322, http://dx.doi.org/10.1016/j.robot.2013.08.004.

[7] I. Vallivaara, J. Haverinen, A. Kemppainen, J. Roning, Magnetic field-based SLAM method for solving the localization problem in mobile robot floor-cleaning task, 15th International Conference on Advanced Robotics (ICAR), IEEE, 2011, , http://dx.doi.org/10.1109/icar.2011.6088632.

[8] J. Fink, V. Bauwens, F. Kaplan, P. Dillenbourg, Living with a vacuum cleaning robot, Int. J. Soc. Robot. 5 (3) (2013) 389–408, http://dx.doi.org/10.1007/s12369-013-0190-2.

[9] D. Sakamoto, K. Honda, M. Inami, T. Igarashi, Sketch and run: a stroke-based interface for home robots, In Proceedings of the 27th International Conference on Human Factors in Computing Systems - CHI 09, ACM Press, 2009, , http://dx.doi.org/10.1145/1518701.1518733.

[10] C. Luo, S.X. Yang, A real-time cooperative sweeping strategy for multiple cleaning robots, Proceedings of the IEEE Internatinal Symposium on Intelligent Control, 2002, IEEE, February 06 2003, http://dx.doi.org/10.1109/isic.2002.1157841.

[11] A. Janchiv, D. Batsaikhan, G. hwan Kim, S.G. Lee, Complete coverage path planning for multi-robots based on, Control, Automation and Systems (ICCAS), 11th International Conference on, IEEE, 2011, October, pp. 824–827 (ISBN: 9788993215038).

[12] S. Rhim, J.-C. Ryu, K.-H. Park, S.-G. Lee, Performance evaluation criteria for autonomous cleaning robots, 2007 International Symposium on Computational Intelligence in Robotics and Automation, IEEE, 2007, http://dx.doi.org/10.1109/cira.2007.382916.

[13] S.C. Wong, L. Middleton, B.A. MacDonald, N. Auckland, Performance metrics for robot coverage tasks, Proceedings of Australasian Conference on Robotics and Automation, Vol. 27 2002, November, p. 29 (ISBN: 0-909040-90-7).

[14] K. Zheng, G. Chen, G. Cui, Y. Chen, F. Wu, X. Chen, Performance metrics for coverage of cleaning robots with mocap system, Intelligent Robotics and Applications, Springer International Publishing, 2017, pp. 267–274, , http://dx.doi.org/10.1007/978-3-319-65298-6_25.

[15] E. Prassler, M. Hägele, R. Siegwart, International contest for cleaning robots: fun event or a first step towards benchmarking service robots, Field and Service Robotics, Springer Berlin Heidelberg, 2003, January, pp. 447–456, , http://dx.doi.org/10.1007/10991459_43.

[16] N. Tan, N. Rojas, M.R. Elara, V. Kee, R. Sosa, Nested reconfigurable robots: theory, design, and realization, Int. J. Adv. Robot. Syst. 12 (7) (2015) 110, http://dx.doi.org/10.5772/60507.

[17] Y. Sun, S. Ma, ePaddle mechanism: towards the development of a versatile amphibious locomotion mechanism, 2011 IEEE/RSJ International Conference on Intelligent Robots and Systems, IEEE, 2011, http://dx.doi.org/10.1109/iros.2011.6095135.

[18] G. WEI, J.S. DAI, S. WANG, H. LUO, Kinematic analysis and prototype of a metamorphic anthropomorphic hand with a reconfigurable palm, Int. J. Humanoid Rob. 8 (3) (2011) 459–479, http://dx.doi.org/10.1142/s0219843611002538.

[19] S. Nansai, N. Rojas, M.R. Elara, R. Sosa, Exploration of adaptive gait patterns with a reconfigurable linkage mechanism, 2013 IEEE/RSJ International Conference on Intelligent Robots and Systems, IEEE, 2014, http://dx.doi.org/10.1109/iros.2013.6697027.

[20] N. Chadil, M. Phadoongsidhi, K. Suwannasit, P. Manoonpong, P. Laksanacharoen, A reconfigurable spherical robot, 2011 IEEE International Conference on Robotics and Automation, IEEE, 2011, http://dx.doi.org/10.1109/icra.2011.5979756.

[21] H. Wei, N. Li, Y. Tao, Y. Chen, J. Tan, Docking system design and self-assembly control of distributed swarm flying robots, Int. J. Adv. Robot. Syst. 9 (5) (2012) 186, http://dx.doi.org/10.5772/53233.

[22] H. Wei, Y. Cai, H. Li, D. Li, T. Wang, Sambot: a self-assembly modular robot for swarm robot, 2010 IEEE International Conference on Robotics and Automation, IEEE, 2010, http://dx.doi.org/10.1109/robot.2010.5509214.

[23] S. Mintchev, C. Stefanini, A. Girin, S. Marrazza, S. Orofino, V. Lebastard, F. Boyer, An underwater reconfigurable robot with bioinspired electric sense, 2012 IEEE International Conference on Robotics and Automation, IEEE, June 28 2012, http://dx.doi.org/10.1109/icra.2012.6224956.

[24] J. Zhao, X. Cui, Y. Zhu, S. Tang, A new self-reconfigurable modular robotic system UBot: multi-mode locomotion and self-reconfiguration, 2011 IEEE International Conference on Robotics and Automation, IEEE, August 15 2011, http://dx.doi.org/10.1109/icra.2011.5980293.

[25] V. Kee, N. Rojas, M.R. Elara, R. Sosa, Hinged-tetro: a self-reconfigurable module for nested reconfiguration, 2014 IEEE/ASME International Conference on Advanced Intelligent Mechatronics, IEEE, 2014, , http://dx.doi.org/10.1109/aim.2014.6878302.

[26] S.W. Golomb, Checker boards and polyominoes, Am. Math. Mon. 61 (10) (1954) 675, http://dx.doi.org/10.2307/2307321.

[27] S. Coffin, J. Slocum, What's new in polyomino puzzles and their design, Mathematical Properties of Sequences and Other Combinatorial Structures, Springer, US, 2003, pp. 113–119, , http://dx.doi.org/10.1007/978-1-4615-0304-0_13.

[28] D.A. Klarner, Polylominoes, Handbook of Discrete and Computational Geometry, CRC Press, Inc., 1997, January, pp. 225–240 (ISBN: 0849385245).

[29] G.N. Frederickson, Hinged Dissections: Swinging and Twisting, Cambridge University Press, 2002 (ISBN: 9780521811927).

[30] E.D. Demaine, M.L. Demaine, D. Eppstein, G.N. Frederickson, E. Friedman, Hinged dissection of polyominoes and polyforms, Comput. Geom. 31 (3) (2005) 237–262, http://dx.doi.org/10.1016/j.comgeo.2004.12.008.

[31] E.D. Demaine, M.L. Demaine, J.F. Lindy, D.L. Souvaine, Hinged dissection of polypolyhedra, Lecture Notes in Computer Science, Springer, Berlin Heidelberg, 2005, pp. 205–217 (ISBN: 9783540317111).

[32] R. Sarhangi, Making patterns on the surfaces of swing-hinged dissections, Bridges Leeuwarden Proceedings, 2008, pp. 251–258 (ISBN: 9780966520194).

[33] V. Prabakaran, M.R. Elara, T. Pathmakumar, S. Nansai, hTetro: a tetris inspired shape shifting floor cleaning robot, 2017 IEEE International Conference on Robotics and Automation (ICRA), IEEE, 2017, , http://dx.doi.org/10.1109/icra.2017.79897.